English Version Manual For F. Praktikum

Laser Spectroscopy of Rubidium

Dr. Gouri S. Giri

Version: October 15, 2016

Recommended Reading:
Chapters 1, 2, 4, 5 and sections 3.1, 3.2.2
(To pass the oral examination and perform the experiment)
Chapter 6
(To understand the setup, tasks and data collection)
Prerequisite Knowledge:
- Basic atomic level scheme
- Quantum numbers
- Fine and hyperfine structure
Depending on prior knowledge a preparation time of 2-3 days may be necessary. Beginning of preparation well in advance (not the night before) is highly recommended.

Fakultät IV – Physik
Universität Siegen

Contents

Chapter 1

Emission, Absorption and Linewidth

In this chapter the different types of emission and absorption processes are discussed. The broadening mechanisms of line profiles are also briefly presented. Further details and derivations can be found in ref. [1].

1.1 Absorption, stimulated and spontaneous emission

When an atom is brought into an electromagnetic radiation field, it can interact with the photons of energy $h\nu$, where h is the Planck's constant and ν is the frequency of the photons. If the atom has two energy levels E_1 (ground state) and E_2 (excited state), the atom goes from the ground state to the excited state if the energy of photon is equal to the difference in energy of the two levels:

$$h\nu = E_2 - E_1. \tag{1.1}$$

Such an interaction is known as (stimulated) absorption (Fig. 1.1, left). Einstein showed that the probability per unit time for this absorption process, P_{12} can be written as

$$P_{12} = B_{12}\rho(\nu), \tag{1.2}$$

where B_{12} is the Einstein coefficient of stimulated absorption and $\rho(\nu)$ is the spectral energy density of the electromagnetic radiation field. The latter is given

by Planck's radiation formula:

$$\rho(\nu) = \frac{8\pi\nu^2}{c^3} \frac{h\nu}{e^{h\nu/k_B T} - 1}, \tag{1.3}$$

where c is the velocity of light in vacuum, k_B is the Boltzmann constant and T is the temperature.

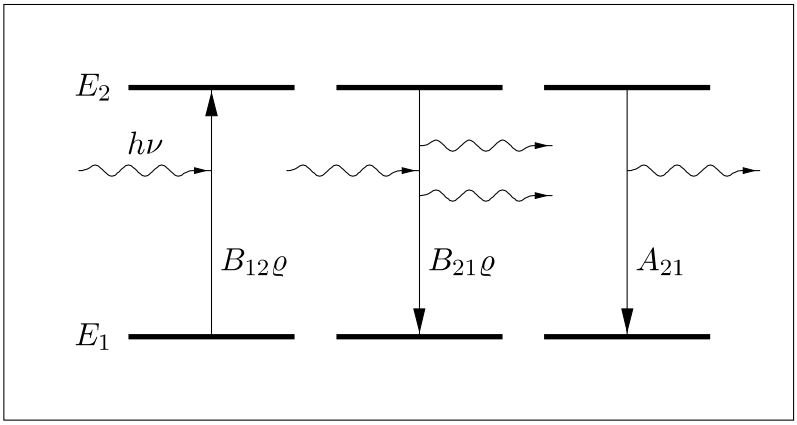

Fig. 1.1: Absorption (left), stimulated emission (center) and spontaneous emission (right) in a two level system. See text for more explanation of these processes.

An atom in the excited state can be stimulated by a photon of frequency ν and return from the excited state to the ground state under emission of a photon of frequency ν. This process is known as stimulated emission (Fig. 1.1, center). The probability P_{21} for this stimulated emission is also proportional to the spectral energy density of the electromagnetic radiation field:

$$P_{21} = B_{21}\rho(\nu), \tag{1.4}$$

where B_{21} is the Einstein coefficient of stimulated emission.

In addition to the spontaneous emission, there is another possibility. The atom can come back to the ground state independently, without being stimulated by an external electromagnetic radiation field. This process depends only on the nature of the atom and is referred to as the spontaneous emission (Fig. 1.1, right). Thus, the probability $P_{21}^{(\mathrm{sp})}$ for this spontaneous emission is given by:

$$P_{21}^{(\mathrm{sp})} = A_{21}, \tag{1.5}$$

where A_{21} is the Einstein coefficient of spontaneous emission. It may be noted that A_{12} does not exit since there is no such phenomenon as spontaneous absorption.

For a large ensemble of atoms in equilibrium, the rate of absorption must be the same as the rate of emission. Therefore,

$$\begin{aligned} N_1 P_{12} &= N_2 \left(P_{21} + P_{21}^{(\mathrm{sp})} \right) \\ \iff N_1 B_{12} \rho(\nu) &= N_2 B_{21} \rho(\nu) + N_2 A_{21}, \end{aligned} \tag{1.6}$$

where N_1 and N_2 are the number density of atoms in the ground and excited state respectively.

1.2 Natural linewidth

An individual atom making a transition between energy levels emits a photon with a well-defined energy/frequency. However, profiles of real spectral lines are not infinitely narrow. Therefore, it is important to see what causes spectral lines to have finite width. It may be noted that energy levels themselves are not infinitely sharp or well defined. Therefore, the emitted photons have a range of frequencies.

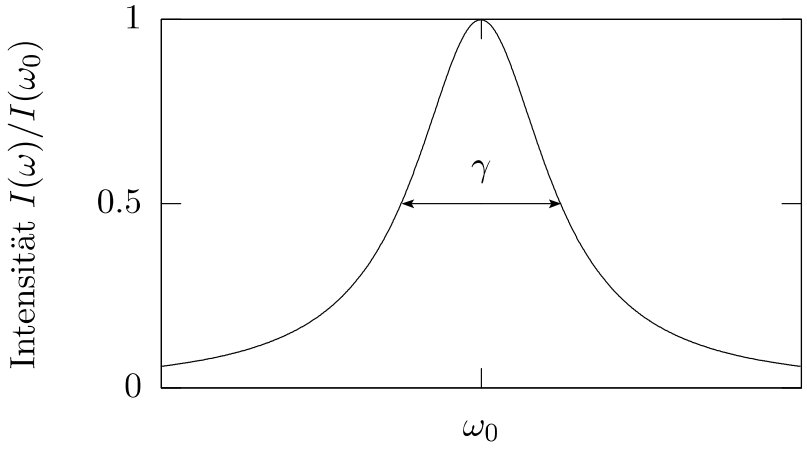

Fig. 1.2: Natural linewidth of a spectral line with a Lorentzian line shape. The horizontal axis represents frequency and the vertical axis represents intensity.

Let's consider an excited state with energy E above the ground state. Electrons in excited state remain there for a finite average time Δt before decaying to ground state. Due to Heisenberg's uncertainty principle, energy of a level is uncertain by an amount ΔE given by:

$$\Delta E \approx \frac{\hbar}{\Delta t}. \tag{1.7}$$

But since $E = \hbar\omega$ or $\Delta E = \hbar\Delta\omega$, width of a spectral line is given by:

$$\Delta\omega \approx \frac{1}{\Delta t}. \tag{1.8}$$

Broadening due to this effect is called the natural linewidth (Fig. 1.2) which depends on the spectroscopic property of the atom itself.

In the absence of all other broadening mechanisms, a spectral line with transition frequency ω_0 has a Lorentzian shape:

$$I(\omega) = I_0 \frac{\gamma/2\pi}{(\omega - \omega_0)^2 + (\gamma/2)^2}, \tag{1.9}$$

where $\gamma = \Delta\omega$ is the Full Width at Half Maximum (FWHM).

1.3 Broadening of spectral lines

Line shapes provide information not only on lifetime, but also on temperature and pressure. Therefore it is important to understand the line shapes and the broadening mechanisms. In our experimental setup the Rubidium atoms are in the form of gas and therefore they are not at rest. Random thermal motion of atoms creates a Doppler shift in the emitted or absorbed radiation. The spectral lines of such atoms are said to be Doppler broadened since the frequency of the radiation emitted or absorbed depends on the velocities of atoms. Individual spectral lines may not be resolved due to Doppler broadening, and hence, subtle details in the atomic structure are not revealed.

We first consider the Doppler effect qualitatively. If an atom is moving toward or away from a laser light source, then it "sees" radiation that is blue or red shifted, respectively. If an atom at rest (relative to the laser) absorbs radiation of frequency ω_0, then the atom approaching the laser will see it as a blue-shifted radiation. Hence, for absorption to occur, the frequency of the laser must be less than ω_0 in order for it to be blue-shifted to the resonance value of ω_0. Similarly, if the atom is receding from the laser, the laser frequency must be greater than ω_0 for absorption to occur.

We now offer a more quantitative argument of the Doppler effect and atomic resonance, where ω_0 is the atomic resonance frequency when the atom is at rest. If the atom is moving along the z axis, say, relative to the laser with $v_z << c$, then the frequency of the absorbed radiation in the rest frame of the laser will be ω_L:

$$\omega_L = \omega_0(1 + \frac{v_z}{c}). \tag{1.10}$$

If v_z is negative (motion toward the laser) then $\omega_L < \omega_0$, that is, the atom moving toward the laser observes radiation that is blue-shifted from ω_L up to ω_0. If v_z is positive (motion away from the laser) then $\omega_L > \omega_0$, that is, the atom observes radiation that is red-shifted from ω_L down to ω_0. Therefore, an ensemble of atoms having a distribution of velocities will absorb light over a range of frequencies. Doppler-shifted frequencies show a Gaussian shape.

$$I(\omega) = I(\omega_0) \exp\left[-\left(\frac{\omega - \omega_0}{\delta\omega_{\mathrm{D}}/2\sqrt{\ln 2}}\right)^2\right]. \tag{1.11}$$

The resulting linewidth,

$$\delta\omega_D = \frac{\omega_0}{c}\sqrt{\frac{8k_BT\ln 2}{m}}, \tag{1.12}$$

is much larger compared to the natural linewidth γ. Here k_B, T and m are the Boltzmann constant, temperature and atomic mass respectively. If the natural linewidth is included together with the Doppler width, a convolution of the Lorentzian into the Gaussian shape can be done, which leads to a so-called Voigt profile (Fig. 1.3).

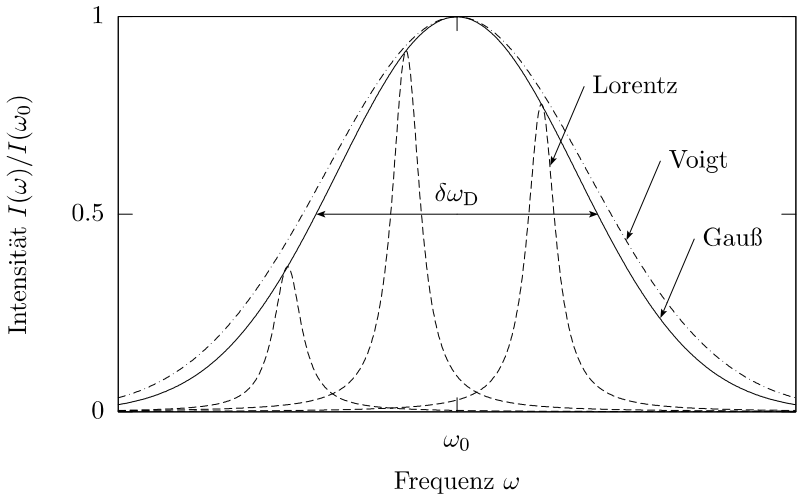

Fig. 1.3: Doppler broadening of a spectral line. The Lorentzian, Gaussian and Voigt (convolution of Lorentzian and Gaussian) profiles are shown. The horizontal axis represents frequency and the vertical axis represents intensity.

There are several other mechanisms that can result in the broadening of a spectral line, such as collisional/pressure broadening, saturation/power broadening etc. Detailed explanation and mathematical treatment about these can be found in ref. [1].

Chapter 2

Laser Spectroscopy

The following two methods of laser spectroscopy are discussed with which the hyperfine splitting of the D2 line of rubidium (see chapter 4) are to be measured. This chapter is adapted from [1]. An additional recommended source of information is [3, Chapter 11].

2.1 Linear absorption spectroscopy

In linear absorption spectroscopy, an atomic sample (in our experiment, atomic rubidium vapor) is examined while a tunable single-mode laser beam (see section 3.2) shines through it. The frequency of the laser is continuously varied and the intensity of the transmitted beam is measured with a photodiode.

For each allowed transition from a ground state to an excited state, an absorption line with Doppler broadening occurs, as described in section 1.3. The twelve allowed transitions of rubidium atom can not all be resolved separately by this spectroscopy method, because at room temperature the Doppler broadening with a line width of $\delta\omega_{\mathrm{D}} \sim 1\mathrm{GHz}$ is significantly greater than the frequency spacing between absorption lines (see Fig. 4.1). This results in a strong overlap of the absorption lines.

However, transitions can be distinguished by the four ground levels due to the large isotope shift (see Fig. 4.2), which is greater than the Doppler width. Thus we measure four absorption lines with Gaussian-like profile, each consisting of a superposition of three lines with Doppler broadening.

In order to improve the measurement signal the laser beam is split into two partial beams of approximately same intensity (using a 50:50 beam splitter) before

passing through the gas cell containing the atomic sample. One serves as the probe beam and the other as a reference beam. Only the probe beam is sent through the gas cell and the difference in the intensity of both beams are measured. Therefore, only the actual absorbed intensity is measured (see Fig. 2.1, upper spectrum).

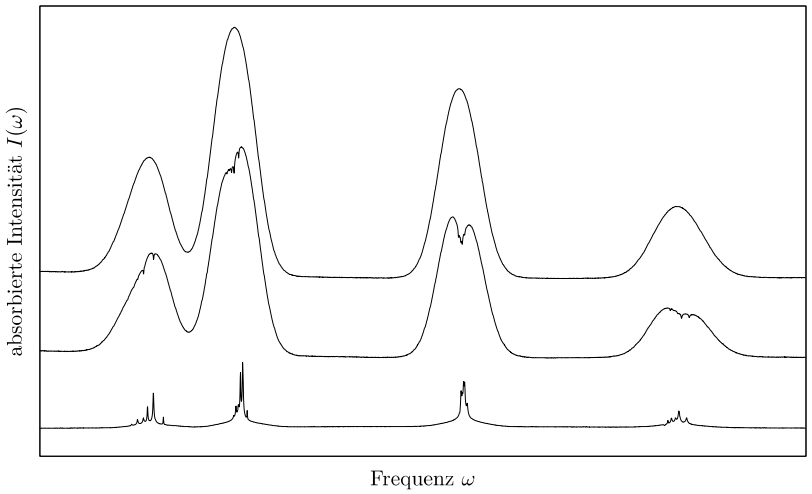

Fig. 2.1: Spectra of the D2 line of rubidium: Absorption Spectroscopy (above), saturation spectroscopy with Doppler background (center), saturation spectroscopy without Doppler background (below). The horizontal axis represents laser frequency and the vertical axis represents absorbed intensity.

2.2 Saturated absorption spectroscopy

The saturation spectroscopy allows us to resolve the lines that are not distinguishable in linear absorption spectroscopy due to the overlap of their Doppler broadened profiles. In this method the laser beam is split into two beams of unequal intensities using a beam splitter (for example, a wedge-shaped glass plate). One is a weak probe beam with about 4-5% of the total intensity of the laser beam and a stronger pump beam with the remaining intensity. Both beams are overlapped in opposite directions while they pass through the gas cell. Similar to the linear absorption spectroscopy the signal of the probe beam is measured as a function of the laser frequency. A very simple schematic of this method is shown in Fig. 2.2.

Let's consider atoms with two levels and a resonance frequency ω_0. If we block the pump beam and let the probe beam only go through the gas cell, then we

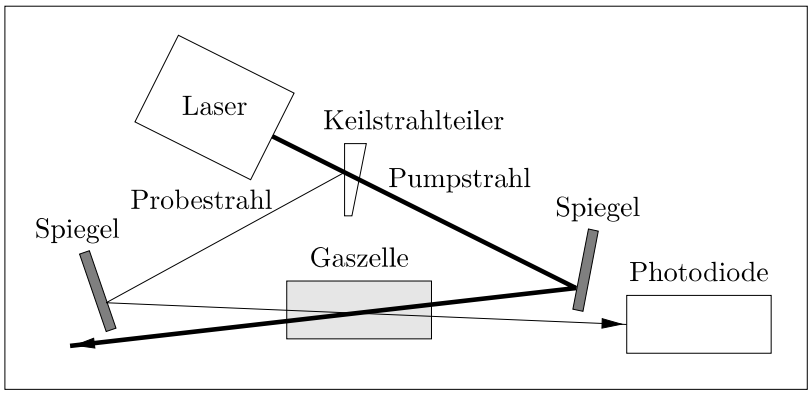

Fig. 2.2: Schematic diagram for saturation absorption spectroscopy. German terms: spiegel = mirror, strahl = beam, zell = cell, keilstrahlteiler = wedge beam splitter.

can observe the absorption lines that are identical to the ones observed in linear absorption spectroscopy (Fig. 2.1, upper spectrum). But if we allow the pump beam to go through the gas cell in addition to the probe beam, a very narrow indentation with Lorentzian profile appears in the probe beam signal at the resonance frequency ω_0, as shown in Fig. 2.3.

It is very important to understand here why such a narrow dip appears in the signal. According to equation 1.10 in section 1.3, the atoms with zero velocity (v_z=0) see both the pump and probe beams as having the same frequency. But the atoms with non-zero velocity ($v_z \neq 0$) see both pump and probe beams as Doppler shifted due to the Doppler effect (see Fig. 2.2). For example, atoms moving to the left will see the pump and probe beams as red-shifted and blue-shifted right respectively. For atoms moving to the right, the Doppler shift for the pump and probe beams will be the other way around.

Due to the high intensity, the pump beam with frequency ω_L essentially excites all atoms with velocity

$$v_z = \frac{(\omega_L - \omega_0)\, c}{\omega_0},$$

which is derived from equation 1.10. Since the probe beam is counter propagating to the pump beam, the former leads to absorption for all atoms with velocity $-v_z$. Therefore, the absorption signal remains unchanged compared to the linear absorption spectroscopy. But when the laser frequency is on resonance ($\omega_L = \omega_0$), the atoms with v_z=0 are excited by the highly intense pump beam so that the ground state is significantly depleted. Therefore, the rate of absorption for the probe beam is reduced, resulting in a narrow dip which has a Lorentzian profile

due to the absence of Doppler shift at resonance. This phenomenon is called hole burning and is shown in Fig. 2.3 and also in the centre spectrum of Fig. 2.1.

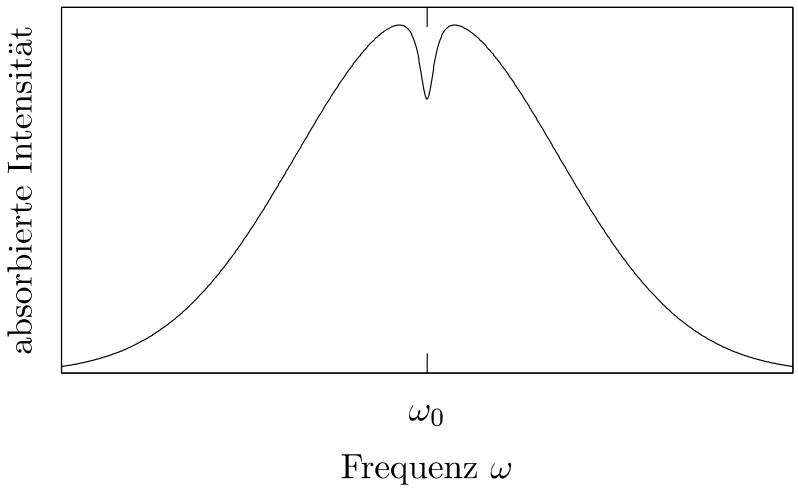

Fig. 2.3: Saturation peak in the Doppler-broadened profile of a two-level atom. The horizontal axis represents laser frequency and the vertical axis represents absorbed intensity.

For a multi-level atom (such as rubidium) the Doppler-broadened absorption lines in the spectrum (see Fig. 2.1, middle) have more indentations due to more transitions and crossover signals [1, S. 349f]. To have a better understanding of these signals, let's consider a three level atom. If the pump beam has a frequency of ω_{01} or ω_{02}, two saturation peaks occur due to the depletion of atoms of velocity $v_z = 0$. But when the laser frequency reaches the average of these two frequencies

$$\omega_{12} = \frac{\omega_{01} + \omega_{02}}{2},$$

the atoms with velocity

$$v_z = \frac{(\omega_{12} - \omega_{01})\, c}{\omega_{12}} = \frac{(\omega_{02} - \omega_{01})\, c}{2\omega_{12}}$$

are excited with frequency ω_{02} by the pump beam and with frequency ω_{01} by the probe beam. Similarly, atoms with velocity $-v_z$

$$-v_z = \frac{(\omega_{12} - \omega_{02})\, c}{\omega_{12}} \quad \Longleftrightarrow \quad v_z = \frac{(\omega_{02} - \omega_{01})\, c}{2\omega_{12}},$$

are excited with frequency ω_{01} by the pump beam and with frequency ω_{02} by the probe beam. Because of the partial depletion of atoms by the pump beam in

both cases, they cannot absorb the frequency of the probe beam and this results in an additional dip in the absorption spectrum. This is called a crossover peak (Fig. 2.4) and is generally larger compared to the respective saturation peaks since atoms of two different velocity classes interact with the laser beam.

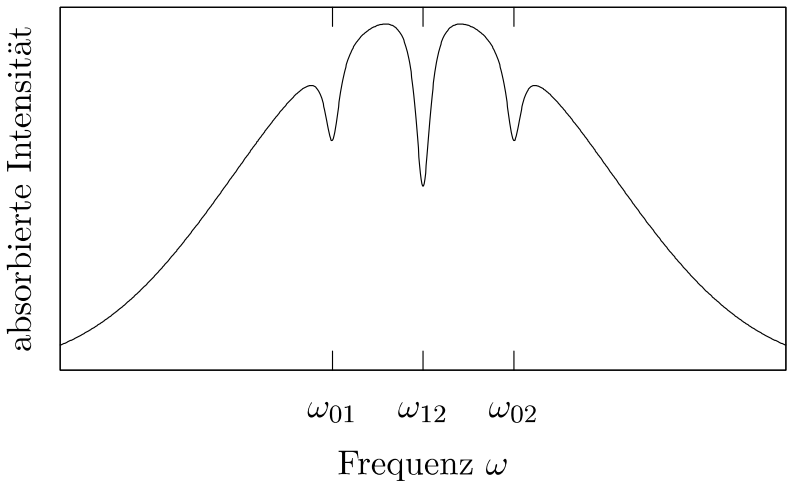

Fig. 2.4: Saturation peaks and crossover signal in the spectrum of three-level atoms. The horizontal axis represents laser frequency and the vertical axis represents absorbed intensity.

It is possible to completely eliminate the Doppler background by measuring the difference between the normal and saturated absorption as shown in the lower spectrum of Fig. 2.1. This leads to a clear resolution of all the accessible transitions in our experiment.

Chapter 3

Semiconductor Lasers and Optical Components

In this chapter, important components of the experimental setup are discussed.

3.1 Fabry-Pérot interferometer

In a confocal Fabry-Pérot interferometer, two spherical mirrors S_1 and S_2 with radii of curvature $r = 2f$ and reflectivity R (or transmission $T = 1 - R$) are arranged in a way that their focal points coincide at F (Fig. 3.1). In general, reflectivity of S_1 (input mirror) is higher compared to that of S_2 (output mirror).

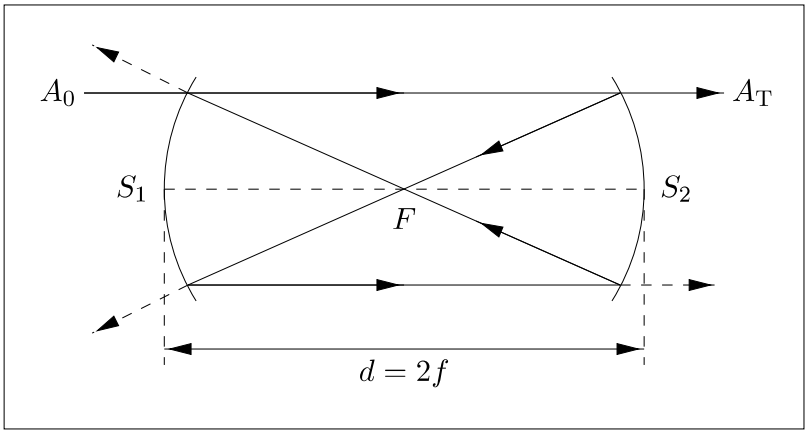

Fig. 3.1: Schematic diagram of a confocal Fabry-Pérot interferometer. See text for more explanation of the symbols and principle of operation.

When an incoming light beam with amplitude A_0 enters the Fabry-Pérot inter-

ferometer and hits mirror S_2, a small part of it is transmitted and the rest is reflected. The reflected beam hits mirror S_1, where again a very small part of the beam is transmitted and the rest is reflected. Therefore, the transmitted beam with amplitude A_T exiting the interferometer in direction of the incident beam is composed of the directly transmitted beam and a $2j$-times reflected beam (j = 0, 1, 2, ...). This is illustrated in Fig. 3.1.

If the input light wave has amplitude A, the amplitude of the reflected wave is $\sqrt{R}A$ and that of the transmitted wave is $\sqrt{T}A = \sqrt{1-R}A$. Therefore, the amplitude of the transmitted wave that leaves the interferometer in the beam direction after j passes is dropped to

$$A_j = TR^{2j}A_0 = (1-R)R^{2j}A_0. \tag{3.1}$$

The reflected part of the output beam has a longer path length of $s_j = 4jd$ compared to the directly transmitted part. This induces a phase shift($\Delta\phi_j$) of the light wave

$$\Delta\phi_j = \frac{2\pi s_j}{\lambda} = \frac{s_j\omega}{c} = \frac{4d\omega}{c}j, \tag{3.2}$$

where $\omega = 2\pi\nu$ is the angular frequency of the light beam and it is assumed that the refractive index of air $n_\mathrm{air} = 1$.

From equations 3.1 and 3.2, the amplitude of the transmitted beam can be expressed as

$$A_\mathrm{T} = \sum_{j=0}^{\infty} A_j e^{i\Delta\phi_j} = A_0(1-R)\sum_{j=0}^{\infty}\left(R^2e^{i4d\omega/c}\right)^j = \frac{A_0(1-R)}{1-R^2e^{i4d\omega/c}}. \tag{3.3}$$

Since the intensity of the light beam is related to the amplitude of the wave by $I(\omega) \propto |A_\mathrm{T}|^2$, therefore, the transmitted intensity of the Fabry-Pérot interferometer is described by the Airy function

$$I(\omega) = I_0\frac{(1-R)^2}{1-2R^2\cos(4d\omega/c)+R^4}, \tag{3.4}$$

which is graphically illustrated in Fig. 3.2.

It may be noted that the Fabry-Pérot interferometer transmits only light with frequencies that are multiples of a specific frequency ω_FSR. This frequency $\nu_\mathrm{FSR} = \omega_\mathrm{FSR}/2\pi$ is called the free spectral range (FSR) and is defined as the distance between two consecutive peaks (transmission maxima or cavity modes) as shown

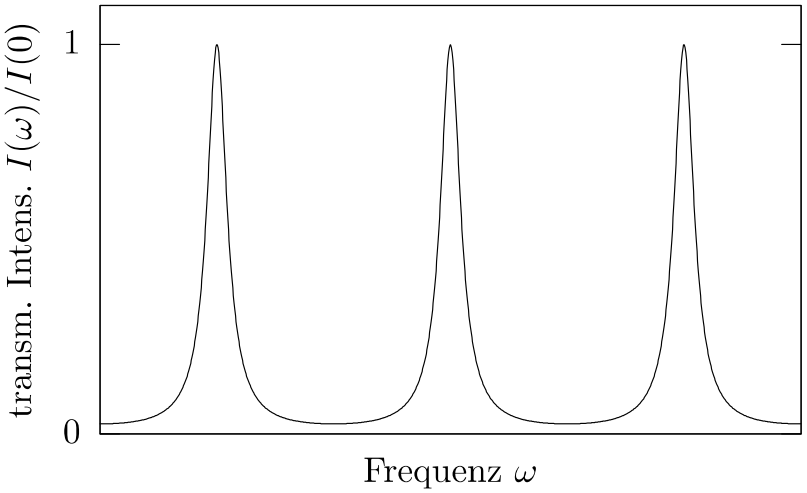

Fig. 3.2: Transmitted intensity of a confocal Fabry-Pérot interferometer. The horizontal axis represents laser frequency and the vertical axis represents transmitted intensity.

in Fig. 3.2. One can see it as the periodicity of cosine in the denominator of equation 3.4:

$$\omega_{\mathrm{FSR}} = \frac{2\pi c}{4d} \quad \Longrightarrow \quad \nu_{\mathrm{FSR}} = \frac{c}{4d}. \tag{3.5}$$

The full width at half maximum for each transmission maximum is given by

$$\omega_{\mathrm{FWHM}} = \frac{c}{d} \arcsin\left(\frac{1-R^2}{2R}\right) \approx \frac{c}{d}\frac{1-R^2}{2R}. \tag{3.6}$$

From equations 3.5 and 3.6 the ratio of ω_{FSR} and ω_{FWHM} can be determined. This ratio is defined as the Finesse F of the Fabry-Pérot interferometer .

$$F = \frac{\omega_{\mathrm{FSR}}}{\omega_{\mathrm{FWHM}}} = \frac{\pi R}{1-R^2}, \tag{3.7}$$

which is a measure of the frequency resolution. Theoretically, the finesse is dependent on the reflectivity of the mirrors, as given in equation 3.7.

3.2 Semiconductor laser

LASER is the acronym for Light Amplification by Stimulated Emission of Radiation. As shown in Fig. 1.1 and described in section 1.1, amplification occurs due to the fact that stimulation by one photon leads to emission of two photons of the same energy. Semiconductor lasers are lasers based on a semiconductor gain medium where optical gain is achieved by stimulated emission.

3.2.1 General working principle

The population density of atoms in the ground state (N_1) is generally more than that in the excited state (N_2). But if the process of stimulated emission dominates over the process of spontaneous emission, then the population density of atoms in the excited state will be higher compared to that in the ground state. This is called population inversion ($N_2 > N_1$).

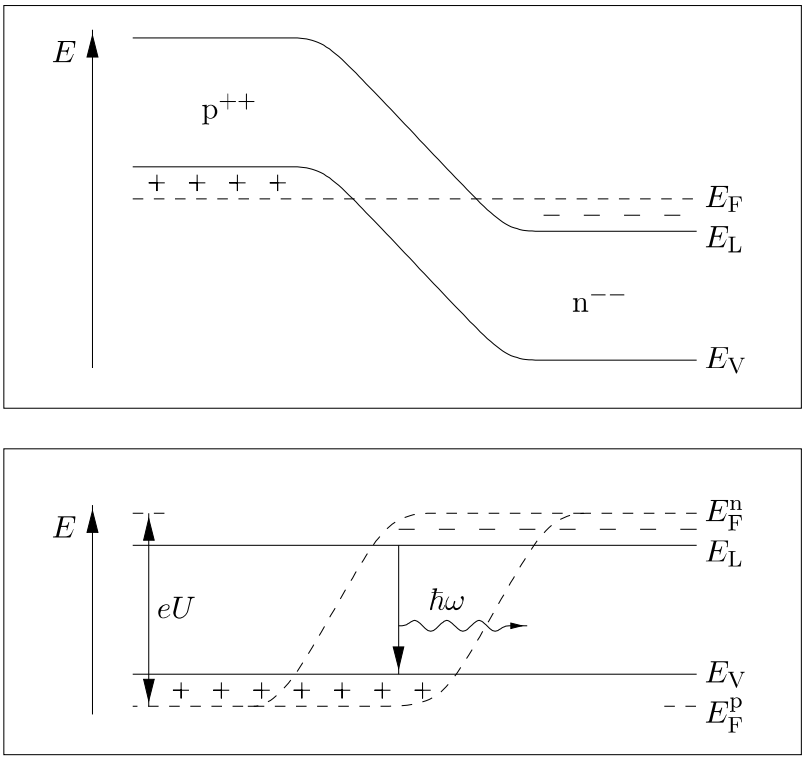

Fig. 3.3: Band diagram of a p^{++} - n^{--} structure without external voltage (top) and with maximum external voltage in the forward direction (down). In both figures Fermi level is shown with the conduction and valence bands. See text for further explanation on laser action.

In a $p-n$ junction diode a forward bias voltage (U) can be used to shift the Fermi levels ($E_{\mathrm{F}}^{\mathrm{p}}$ and $E_{\mathrm{F}}^{\mathrm{n}}$) of the $p-$ and $n-$ doped semiconductors in a way that the total shift is greater than the band gap ($E_{\mathrm{g}} = E_{\mathrm{L}} - E_{\mathrm{V}}$) of the undoped semiconductor

$$E_{\mathrm{F}}^{\mathrm{n}} - E_{\mathrm{F}}^{\mathrm{p}} > E_{\mathrm{L}} - E_{\mathrm{V}},$$

where E_{L} and E_{V} represent the energy of the conduction band and valence band respectively.

This results in the injection of electrons into the conduction band along n-side and the production of more holes in the valence band along p-side of the junction. So there will be more number of electrons in the conduction band than that in the valence band. This is how population inversion is achieved. When electrons recombine with the holes there will be release of energy in the form of photons. These spontaneously emitted photon during recombination in the junction triggers laser action near the junction diode. This is shown in Fig. 3.3. An optical resonator or cavity is required to achieve stimulated emission and the amplification of the emitted radiation. An optical cavity generally consists of two unequally high reflective mirrors separated by a distance, an arrangement that is very similar to the Fabry-Pérot cavity described in section 3.1. The cavity we are referring to is called an internal cavity. The polished surfaces of the semiconductor material serves as mirrors which are separated by a small distance at the junction. This is shown in Fig. 3.4.

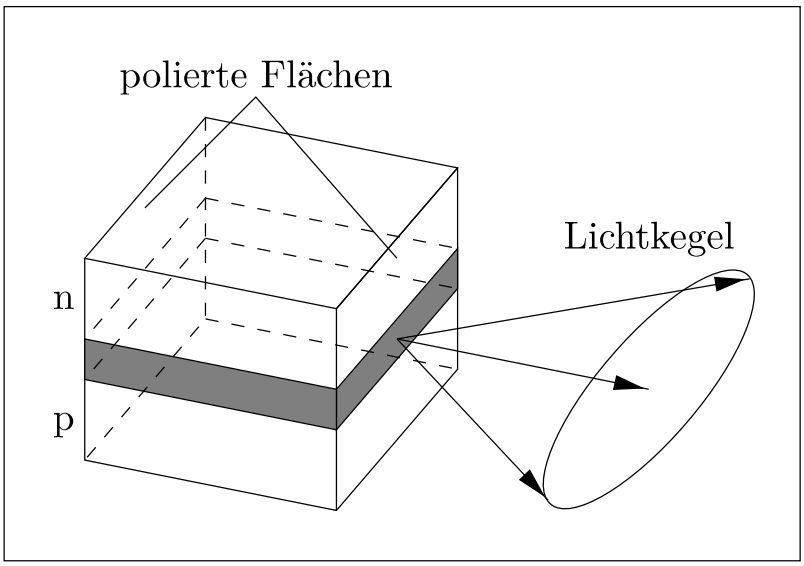

Fig. 3.4: Schematic representation of a laser diode. German terms: polierte flächen = polished surfaces, lichtkegel = light cone.

3.2.2 Littrow configuration

The line width of the semiconductor laser is relatively large (around 100 MHz) due to the short length of the internal resonator and a very low reflectivity of the polished surfaces of the semiconductor [4, Part IV 1.2]. This problem can be

solved by using a diffraction grating in a so called extended cavity diode laser (ECDL) configuration or Littrow configuration. This is schematically shown in Fig. 3.5 and 3.6.

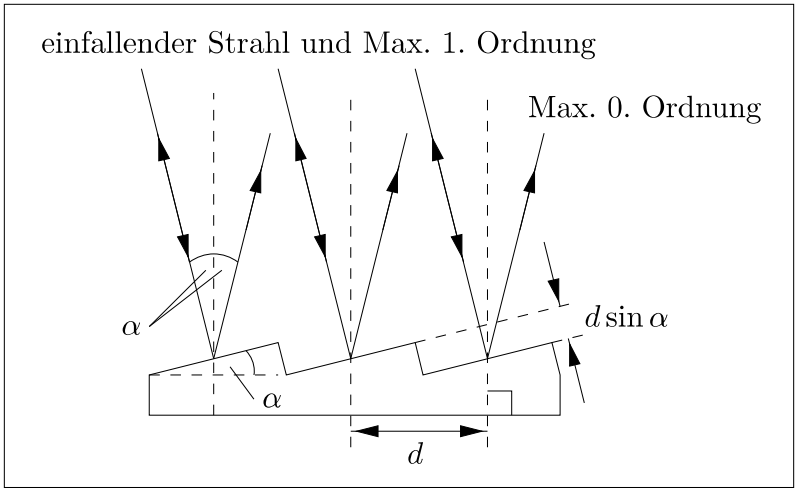

Fig. 3.5: Blazed grating in Littrow configuration. German terms: einfallender strahl = incident beam, or dung = order. See text for further explanation.

The external cavity consists of a diffraction grating that couples part of the light into the laser through the end orifice of the diode (Fig. 3.6). The grating angle is set to reflect light for a particular wavelength in the direction of the incoming light. This is the concept of Littrow configuration. The diffraction angle for a grating in Littrow configuration satisfies the grating equation $2d \sin \alpha = n\lambda$, where d is the groove spacing which is equal to (groove density)$^{-1}$, α is the angle of incidence, n is the order of diffraction, and λ is the wavelength of the incident light (Fig. 3.5). The only wavelengths that satisfy this grating equation are reflected back from the grating. The laser diode is forced to resonate at the wavelength that is fed back from the grating and hence it oscillates at a frequency that is coupled into it. By changing the angle α, the emission frequency of the laser diode can be altered. The 0^{th} order diffraction is coupled out of the external resonator and the -1^{st} order diffraction is coupled into the laser diode. The criteria based on which a grating is generally chosen are that the angle between incident beam and first order diffraction angle should be close to 45°, and the intensity that is coupled back should lie between 20-30%. The efficiency of a grating depends on the total number of illuminated grooves and the polarization of the incident light. The frequency of the lasers in ECDL configuration can be changed by altering the operating current. The frequency can also be changed by altering the external

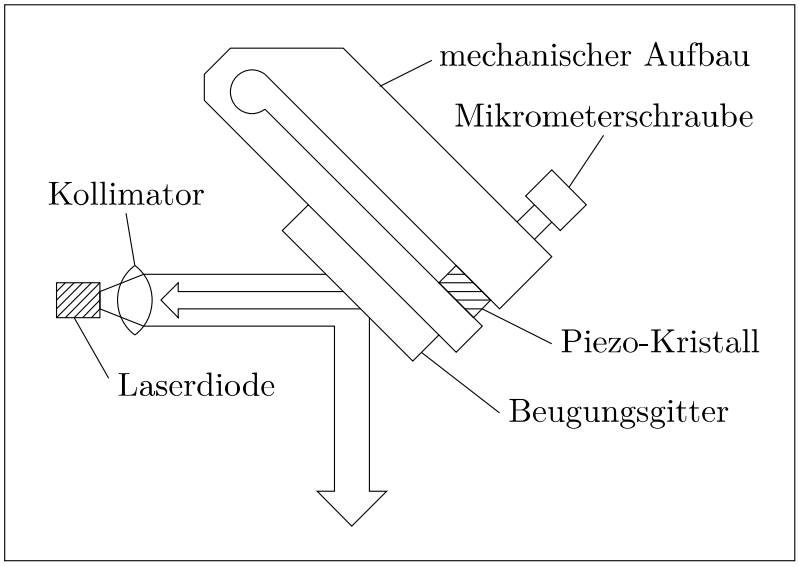

Fig. 3.6: Schematic design of the laser system (see. [4], part IV, 1.3). German terms: kollimator = collimator, mechanischer aufbau = Mechanical design, mikrometerschraube = micrometer screw, piezo-kristall = piezoelectric crystal, beugungsgitter = diffraction grating.

cavity. This can be achieved by changing the temperature of the laser and/or by moving the PZT (piezo electric transducer) mounted grating by varying the voltage applied to the PZT. This alters the angle of incidence α (Fig. 3.5) and hence the emission frequency of the laser changes. The PZT element typically has an extension coefficient of 30(10) nm/V which is a measure of the rate of change of expansion per unit voltage applied. The frequency stabilized laser systems in an experiment can have a long-term stability of about several hours. By altering the PZT-mounted grating element together with the operating current, the frequency of the lasers can be scanned over 10 GHz without any mode hop. A laser in ECDL configuration can have several mod hop free tuning range as shown in Fig. 3.7.

3.3 Optical isolator

In general, each surface reflects a fraction of the incident light back towards the source. For glass surfaces (without anti-reflection coating) the amount of back reflection can be about 4%. A diode laser is very sensitive to back reflections. The latter can cause mode jumps or even destruction of the expensive laser diode. Therefore, as a rule, an optical isolator is mounted immediately after the diode

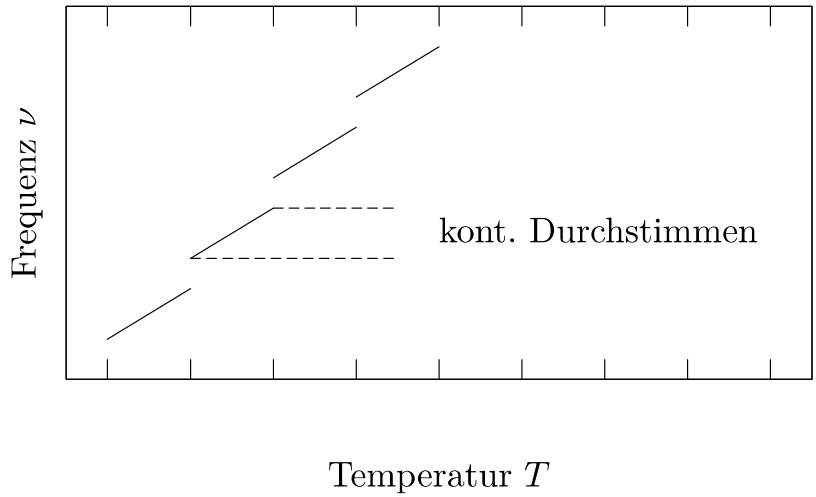

Fig. 3.7: Mode hops during tuning of the temperature. The horizontal axis represents temperature and the vertical axis represents frequency. German term: kont. durchstimmen = continuous tuning.

laser in order for the isolator to allow transmission of light in one direction only. The working principle underlying an optical isolator is the Faraday effect or Faraday rotation. This is magneto-optical phenomenon. In presence of a magnetic field $\vec{B}$, the plane of polarization of light propagating through an optically active substance is rotated (Fig. 3.8). The change in the angle α is proportional to the magnetic field strength B and the length l of the optically active substance:

$$\alpha = VlB, \tag{3.8}$$

where, the proportionality factor V is the Verdet constant of the material and is dependent on wavelength. The sign of the rotation angle α is dependent on whether the light wave propagates along or against the direction of $\vec{B}$. The rotation is counter clockwise (L-rotation) when the direction of propagation is along the magnetic field (parallel) and is clockwise (R-rotation) for propagation against (anti-parallel) the magnetic field. Therefore, the plane of polarization rotates twice when light is passed through the material and is reflected back through it.

An optical isolator consists of two polarizers rotated by 45° (Fig. 3.8). An incident light is initially linearly polarized in the forward direction. Subsequently, the plane of polarization in the Faraday rotator is rotated by 45°. So the light can pass through the second polarizer unhindered. In the backward direction, since the back reflected light is also initially linearly polarized, its plane of polarization

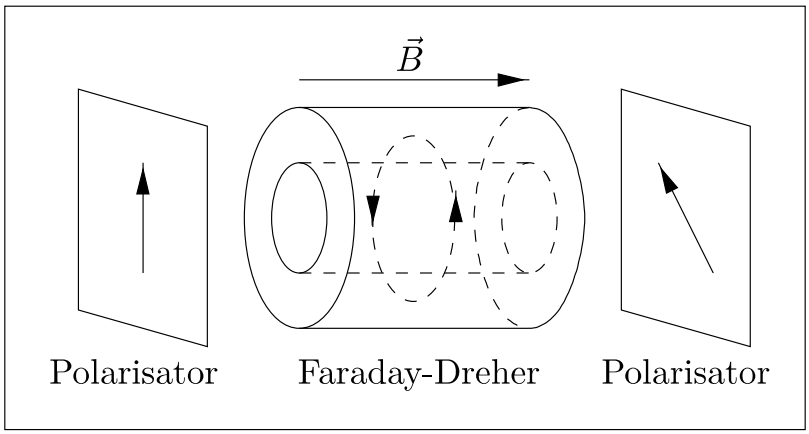

Fig. 3.8: Schematic diagram of an optical isolator. German terms: polarisator = polarizer, dreher = rotator. See text for further explanation.

is rotated by another 45° in the opposite direction. Therefore, the plane of polarization of the back reflected light is perpendicular to the input polarizer and is absorbed.

Since a diode laser in any case emits linearly polarized light, the polarizers of the optical isolator can be rotated accordingly in order to prevent significant intensity attenuation in the forward direction.

3.4 Waveplates

Wave plates are made of anisotropic crystals in which the refractive index n depends on the polarization of the incident light.The axes with extreme refractive indices $n_{\min}$ or $n_{\max}$ are perpendicular. $\lambda/4$ plates are used to generate elliptically polarized light. These are not used in our experiment. With $\lambda/2$ plates, the polarization direction of linearly polarized light can be rotated.

If d is the thickness of the $\lambda/2$ plate, then

$$n_{\max} - n_{\min} = \frac{\lambda}{2d} = \frac{\pi}{kd}. \tag{3.9}$$

The principle of operation of a $\lambda/2$ plate is illustrated in Fig. 3.9. The electric field $\vec{E}$ of a linearly polarized light is decomposed into its component in the direction of the extreme refractive indices, $\vec{e}_{\min}$ and $\vec{e}_{\max}$. The front of the $\lambda/2$-plate is lying at $r = 0$.

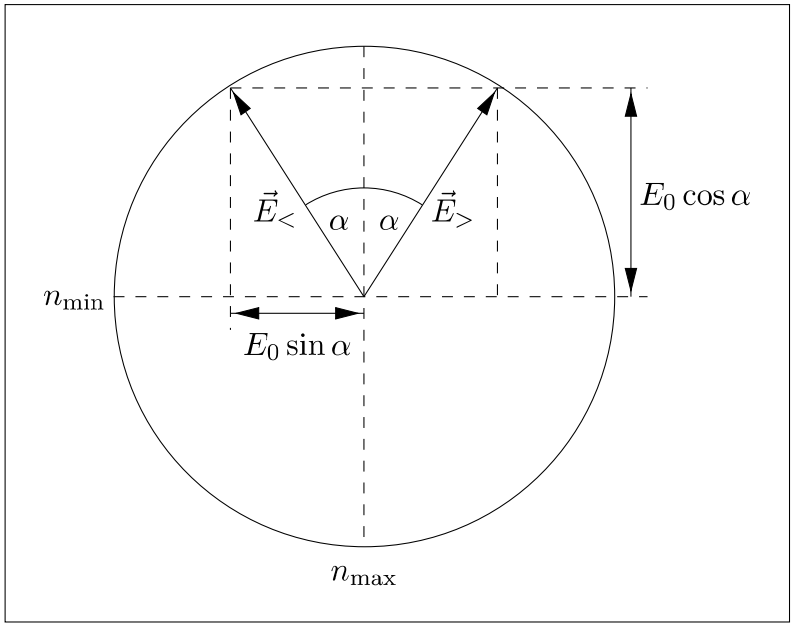

Fig. 3.9: Principal axes of a $\lambda/2$-plate and directions of incoming and outgoing $\vec{E}$ field.

Before passing through the wave plate ($r \ \ le\ 0$), the electric field has the form

$$\vec{E}_< = E_0 \left(\sin\alpha\, \vec{e}_{\min} + \cos\alpha\, \vec{e}_{\max}\right) e^{i(kr-wt)}. \tag{3.10}$$

After emerging on the back of the wave plate ($r \ \ ge\ d$, it has the form

$$\begin{aligned}
\vec{E}_> &= E_0 \left(\sin\alpha\, e^{ikn_{\min}d}\vec{e}_{\min} + \cos\alpha\, e^{ikn_{\max}d}\vec{e}_{\max}\right) e^{i(k(r-d)-wt)} && \text{(3.11a)}\\
&= E_0 \left(\sin\alpha\, e^{-ik(n_{\max}-n_{\min})d}\vec{e}_{\min} + \cos\alpha\, \vec{e}_{\max}\right) e^{ikn_{\max}d} e^{i(k(r-d)-wt)} && \text{(3.11b)}\\
&= E_0 \left(-\sin\alpha\, \vec{e}_{\min} + \cos\alpha\, \vec{e}_{\max}\right) e^{ikn_{\max}d} e^{i(k(r-d)-wt)}. && \text{(3.11c)}
\end{aligned}$$

The above equation suggests that the polarization direction of the light is actually rotated by 2α after passing through the $\lambda/2$ plate.

3.5 Anamorphic prism pair

The light beam emitted by the diode laser usually has an elliptical profile having a ratio of diameters of approximately 1:3. An anamorphic prism pair is mounted immediately after the optical isolator in order to correct the beam profile.

In an exemplary arrangement (Fig. 3.10) the laser beam strikes perpendicular to

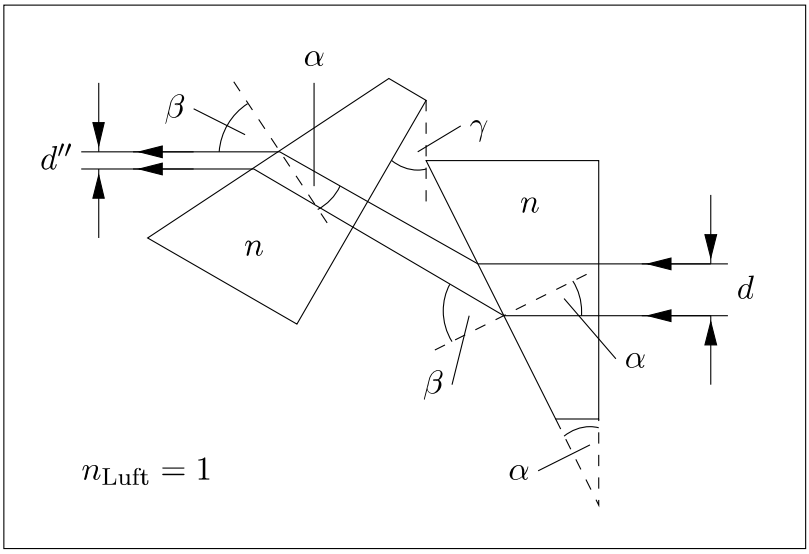

Fig. 3.10: Anamorphic prism pair in the simplest arrangement. German term: luft = air.

the input side of the anamorphic prisms. With the law of refraction,

$$n \sin \alpha = \sin \beta. \tag{3.12}$$

From simple geometric considerations the angle be written as

$$\gamma = \beta - \alpha = \arcsin(n \sin \alpha) - \alpha. \tag{3.13}$$

Hence, the beam width can be expressed as

$$d' = d \cos \gamma \quad \Longrightarrow \quad d'' = d \cos^2 \gamma, \tag{3.14}$$

where d' and d'' are the beam widths after passing through the first and second prisms respectively. With an appropriate prism material with refractive index n and an angle α, the desired factor of $\cos^2 \gamma$ can be achieved.

Chapter 4

Rubidium Atom

4.1 Introduction

Rubidium is an alkali metal which exists in a natural isotopic mixture of about 72% ^{85}Rb and 28% ^{87}Rb. Its melting point is only about 39 °C and its boiling point is about 688 °C. Therefore, gas cells sufficiently filled with rubidium vapour can be used at room temperature. The atomic masses are $m_{\text{Rb-85}} = 84.91$ u and $m_{\text{Rb-87}} = 86.91$ u (see [9]).
The following notation is used to describe the state of an atom,

$$N^{2S+1}L_J$$

where N is the principal quantum number, L is the orbital angular momentum, S is the electron spin and J is the total angular momentum. The quantum numbers in capital letters indicate that they refer to the sum of all orbital electrons. In alkali metals such as rubidium in the ground state, all energy levels are completely occupied except for the singly occupied highest energy level. In spectroscopy, it is a common practice to use $\mathrm{S}, \mathrm{P}, \mathrm{D}, \mathrm{F}, \ldots$ for $L = 0, 1, 2, 3, \ldots$ respectively.

4.2 Fine and hyperfine splitting

The ground state of a rubidium atom is 5S. The first excited is 5P, which is split into $5\mathrm{P}_{1/2}$ and $5\mathrm{P}_{3/2}$ due to spin-orbit coupling (fine structure). To investigate the D1 line which corresponds to the transition $5\mathrm{S}_{1/2} \leftrightarrow 5\mathrm{P}_{1/2}$, light of wavelength 795 nm is required which is not available in our lab. We restrict ourselves to the measurement of the hyperfine splitting of the transition $5\mathrm{S}_{1/2} \leftrightarrow 5\mathrm{P}_{3/2}$ at 780

nm, the D2 line.

The hyperfine splitting occurs due to coupling of the total angular momentum $\vec{J}$ of the electron with the nuclear spin $\vec{I}$. Since the two natural rubidium isotopes have different nuclear spins, namely $I = 5/2$ for ^{85}Rb and $I = 3/2$ for ^{87}Rb, we get two different energy splitting as shown in figures 4.1 and 4.2.

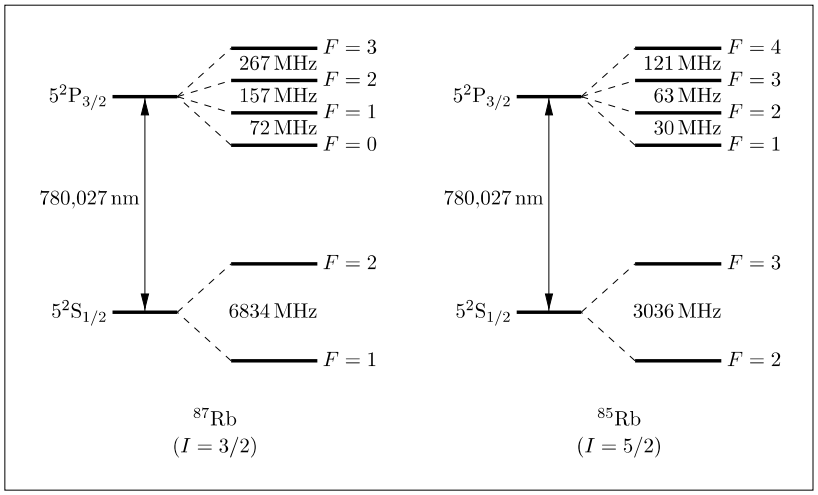

Fig. 4.1: Level schemes of naturally occurring rubidium isotopes.

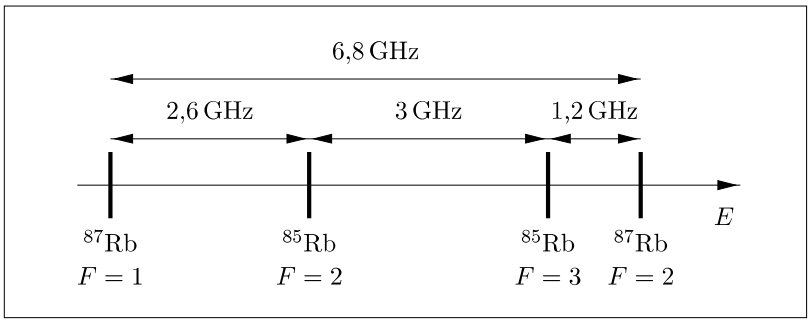

Fig. 4.2: Isotope shift of the D2 line of naturally occurring rubidium isotopes.

The total angular momentum of the atom $\vec{F}$ is given by:

$$\vec{F} = \vec{I} + \vec{J} \implies |I - J| \leq F \leq I + J. \tag{4.1}$$

It follows that with $J \leq I$, the total angular momentum $\vec{F}$ has $2J + 1$ possible values. The energy splitting for a $^{2S+1}L_J$-manifold can be obtained by

$$\nu_F = \nu_J + \frac{AC}{2} + \frac{B\left[\frac{3C(C+1)}{4} - I(I+1)J(J+1)\right]}{2I(2I-1)J(2J-1)}, \tag{4.2}$$

where $C = F(F+1) - J(J+1) - I(I+1)$ and A, B are the hyperfine constants. For (dipole) transitions between the hyperfine energy levels, the selection rules are,

$$\Delta F = 0, \pm 1 \qquad \text{not} \quad (F = 0) \rightarrow (F = 0) \tag{4.3}$$

$$\Delta M_F = 0, \pm 1 \qquad \text{not} \quad (M_F = 0) \rightarrow (M_F = 0) \quad \text{for} \quad \Delta F = 0 \tag{4.4}$$

where the quantum number M_F is the z-component of $\vec{F}$.
In our experiment a total of twelve transitions are accessible, three transitions to various excited hyperfine states from each of the four hyperfine ground states, as shown in Fig. 4.1.

Chapter 5

Quantum Coherence

5.1 Lambda system

First, we set the beam direction as the z axis of quantization. We can have a linearly polarized laser beam as well as a superposition of left (σ_-) and right circularly (σ_+) polarized light. The left circularly polarized photons can drive transitions with $\Delta M_F = -1$ and right circularly polarized photon can drive transitions with $\Delta M_F = 1$.

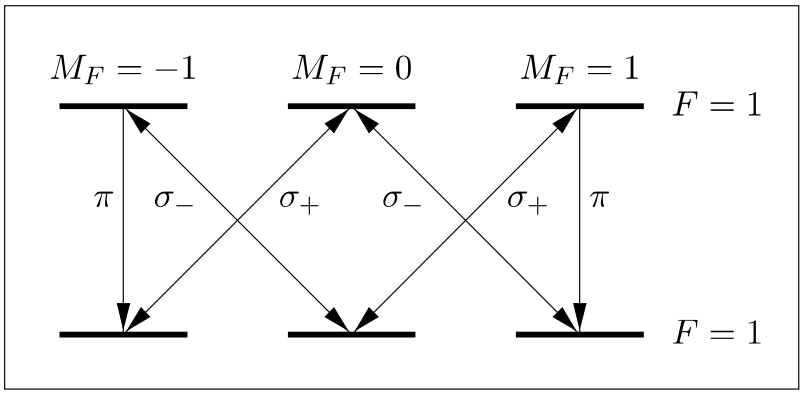

Fig. 5.1: System with triple degeneracy in the ground state and excited state.

Now we look at two levels with $F = 1$ with the threefold degeneracy in the M_F quantum number (see Fig. 5.1). Transitions with $\Delta M_F = 0$ can occur spontaneously, but not induced by the laser, due to the fact that the transition $(M_F = 0) \rightarrow (M_F = 0)$ for $\Delta F = 0$ is forbidden by the selection rule.

We shine laser light on such a system with threefold degeneracy. The electron goes from the ground state $M_F = 0$ to one of the two possible excited states, and then

with a certain probability decays spontaneously with $\Delta M_F = 0$. This process is called optical pumping. Since an electron in the ground states $M_F = \pm 1$ cannot return to the ground state $M_F = 0$, an effective lambda system can exist (see Fig. 5.2). The Lambda system has its name because of the similarity with the Greek letter Lambda.

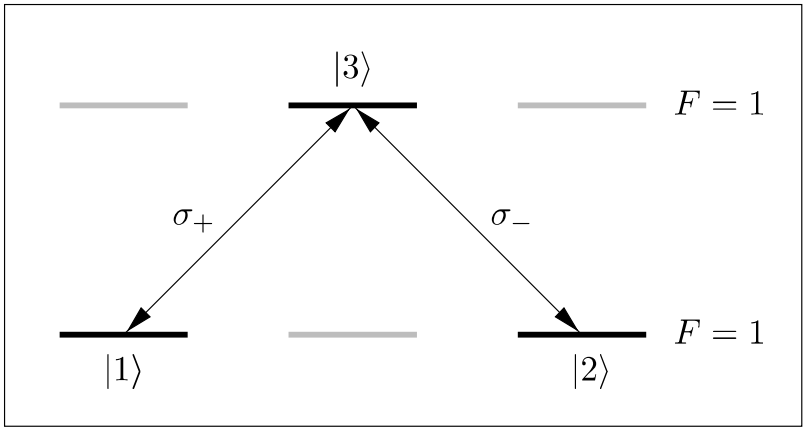

Fig. 5.2: Lambda system.

5.2 Coherent dark states

When we irradiate the system, sometimes it breaks down into an antisymmetric superposition state $|-\rangle = |1\rangle - |2\rangle$, which does not interact with the light. Thus, the matrix element for the transition from $|-\rangle$ to $|3\rangle$ disappears:

$$\langle 3| \vec{d} \cdot \vec{E} |-\rangle = 0. \tag{5.1}$$

Here $\vec{E}$ is the electric field of the light and $\vec{d}$ is the dipole moment operator of the atom. This means that no absorption or emission can take place from the antisymmetric state even though the laser frequency coincides with that of a transition. This is called a coherent dark state. For levels with $F = 2$ such processes occur and the antisymmetric ground state does not interact with the laser beam. With the help of a magnetic field in the z direction, the degenerate ground states can split due to the Zeeman effect and the coherent dark state are destroyed. We exploit this effect for the observation of coherent dark states. The laser frequency is (for example) on the $(F = 1) \rightarrow (F = 1)$ or $(F = 2) \rightarrow (F = 2)$ transition and the absorbed intensity $I(\omega)$ is measured as a function of the magnetic field $\vec{B}$. At $\vec{B} = 0$ the absorbed intensity has a negative peak.

Chapter 6

Experiments and Tasks

Now that all the theoretical foundations needed to understand and carry out the experiment should be adequately explained, we come finally to the experiment.

6.1 Experimental setup

The complete experimental setup demonstrating absorption and saturation spectroscopy is shown in Fig. 6.1. In the top row (from right to left) there are the laser, the optical isolator, the anamorphic prism pair, the gray scale mirror and the telescope. The prism pair is discussed in section 3.5 for beam shaping. The gray scale mirror is essentially a glass cube increasingly strong black colour from left to right. This is used for simple attenuation of the laser beam. The laser beam expands in the telescope to a diameter of about 3 mm. This part should be already adjusted and requires no modification.

Now, the laser beam on the left side is injected to the experiment by splitting roughly 95% of the total intensity at the first wedge beam splitter. The leftover intensity is coupled via a lens and two mirrors into a Fabry-Pérot interferometer in order to verify that the laser is in a single mode and has a frequency scale in the rubidium spectra. The two mirrors before the interferometer are for beam coupling, by opposite rotation of the two screws of the mirror mount. The photodiode with integrated amplifier provides a voltage signal which is proportional to the transmitted intensity.

The experimental beam, the second partial beam of the first wedge beam splitter, is again split by the second wedge beam splitter. For each beam, the intensity is controlled by a $\lambda/2$-plate together with a polarizing beam splitter cube (sec-

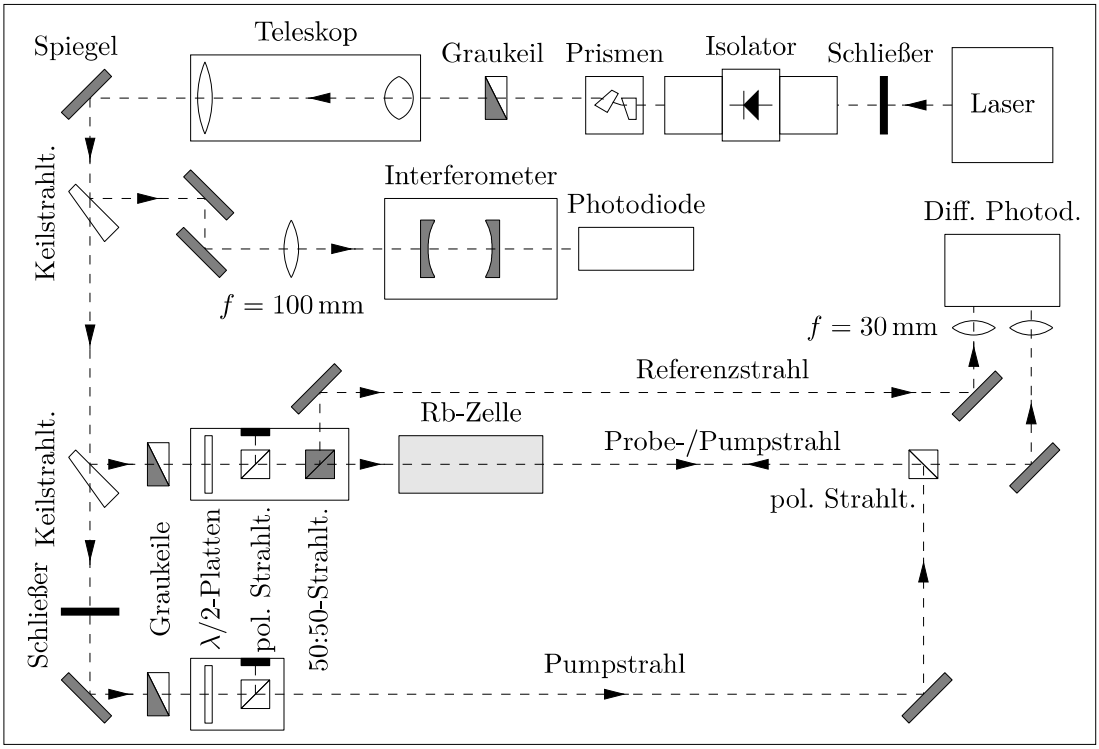

Fig. 6.1: Schematic diagram of the complete experimental setup. German terms: schließer = shutter, prismen = prisms, graukeil = grey scale mirror, telescope = telescope, spiegel = mirror, keilstrahlt = wedge splitter, sell = cell, pol. strahlt = polarizing beam splitter, strahl = beam, referenz = reference. See text and chapter 3 for further explanation.

tion 3.4). The polarizing beam splitter cube is set so that the beam can freely pass through and the polarization is not rotated by the $\lambda/2$-plate. Subsequently, the beam is split (using a non-polarizing 50-50 beam splitter cube) into two partial beams of roughly equal intensity, which are a probe beam passing through a gas cell with rubidium vapor, and a reference beam passing the other direction. The final polarizing beam splitter cube is aligned so that the pump beam can counter-propagate the probe beam. Finally, the probe and reference beams are focused on a differential photodiode, which converts the difference in their intensity with adjustable gain to a voltage signal.

The last part of the main beam is used as a pump beam and, as described previously, this beam also passes through a grey scale mirror and a $\lambda/2$-plate for intensity control. The polarizing beam splitter cube, however, is adjusted so that the polarization of the exiting beam is perpendicular to the probe beam. For this reason, the rightmost polarizing beam splitter cube causes a reflection

of the pump beam by 90° and it is possible to overlap the probe and pump beam optimally.
In the experimental setup, there are two shutters that may block the pump beam or the entire laser beam.

6.2 Experimental procedure

6.2.1 Commissioning of the diode laser

These requirements must be met before starting the laser:

- You must have been told a policy by the laser safety officer.
- Read operating instructions of the laser system available in both manuals.
- Darken windows and doors, so that no radiation can escape from the room.
- Attach label "Laser operation" to the outside of the door.
- Wear protective goggles during the entire operating period. Never, even with goggles, look into the laser beam!
- Never engage with reflective surfaces in the laser beam path. Take off rings, watches, jewelry, etc.

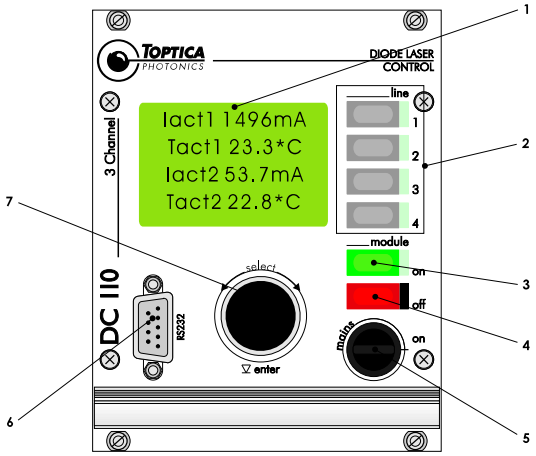

Fig. 6.2: Front panel of monitor unit of the diode laser system (Ref. [4], see part IV, 2.2).

The laser control system consists of a rack, which is equipped with four modules. The first module is the monitor unit (Fig. 6.2), which shows the parameters such as the set current I_{set}, its actual value I_{act} , the set temperature T_{set} , its actual value T_{act}, the maximum current I_{max} etc. shown on the display (1). Furthermore, this module has a key switch (5) and an on (3) or off (4) switch for the laser diode operation.

The second module is the Temperature Control unit (Fig. 6.3, left), which serves for controlling the Peltier element and therefore the temperature stabilization. The adjustment of the temperature is done via the potentiometer (2).

The third module is the current control unit (Fig. 6.3, right) to control the laser diode current . The adjustment of the current is done via the potentiometer (3).

The last module is the scan control unit (Fig. 6.4) which generates a high voltage signal to the piezo-delta crystal for periodically tuning the laser. The amplitude of the voltage, and thus the tuning range of the laser frequency is adjusted by means of potentiometer (2), with the potentiometer (3) the offset of the laser voltage and frequency can be varied, provided that with switch (10) has been switched on.

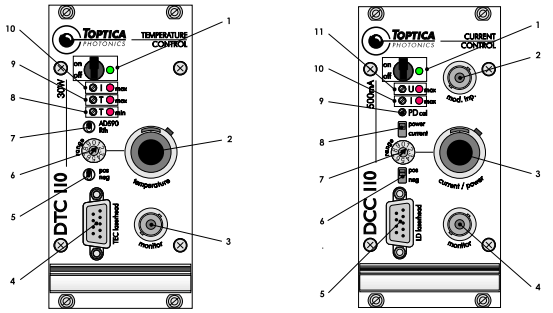

Fig. 6.3: Front panel of temperature (left) and current (right) controller unit of the diode laser system (Ref. [4], see part VII, 2.1 and part VI 2.1).

The operating procedure of the laser system must be addressed as follows:

- Make sure that the shutter next to the diode laser is closed and the exit hole of the diode itself is opened.
- Check that the power switch (1) of all modules and the key switch (5) of the monitor unit is switched off.
- Switching the power switch on the back of the rack.
- Switch on the monitor unit with the key switch.

- Check if a temperature $T_{set} = 20°$ is set. If necessary, set by readjusting at the Temperature Control Unit.
- Switch on the Temperature Control Unit and wait about 10-15 minutes, until the temperature of the diode laser is stabilized.
- Check that a current is set $I_{set} \approx 150$ mA and readjust if necessary.
- Switch on the current control unit.
- Press the modules on switch (3) at the monitor unit.
- Open the shutter in front of the laser diode and check with the infrared card behind the optical isolator, if the laser beam is ready.
- Switch on the Scan Control unit and adjust an amplitude of about 7.

Switching off is done in reverse order.

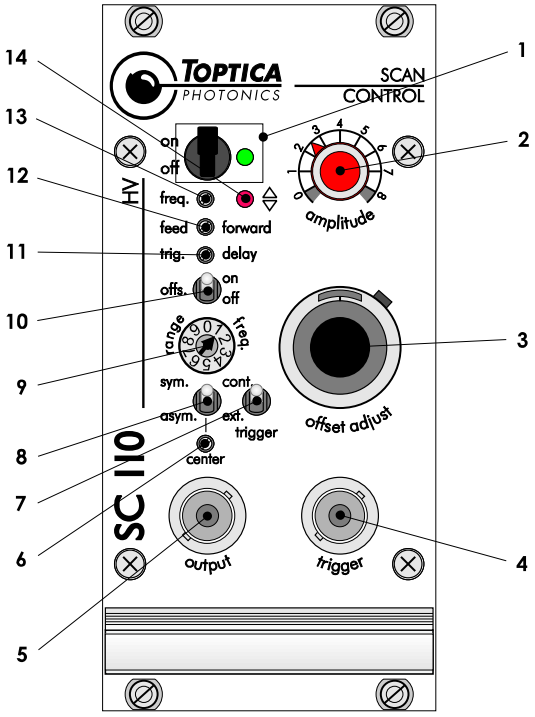

Fig. 6.4: Front panel of scan controller unit of the diode laser system (Ref. [4], see part VIII, 2.1).

Caution: To avoid damaging the laser diode, switches and knobs which are embedded in the front of the module must not be changed! Before the current control module is switched off, first switch off the laser diode with modules on-off switch (4) of the monitor unit! Do not switch off the laser during the experiment!

6.2.2 Description of the photodiodes

For three potentiometers of the simple photodiode (Fig. 6.5, right) the following applies: the signal of the first photodiode isattenuated by a factor $g = 0...1$, then amplified by a factor $G = 1...100$ and finally an offset U_{offs}. (The signal from the photodiode is output inverted!)

Each potentiometer has 20 turns and must only be adjusted with the provided tool (not with a regular screwdriver!). Clockwise causes an increase of the respective value. At the end of a potentiometer, a faint clicking noise could be heard with every other revolution. The gain g should always be set to its maximum value.

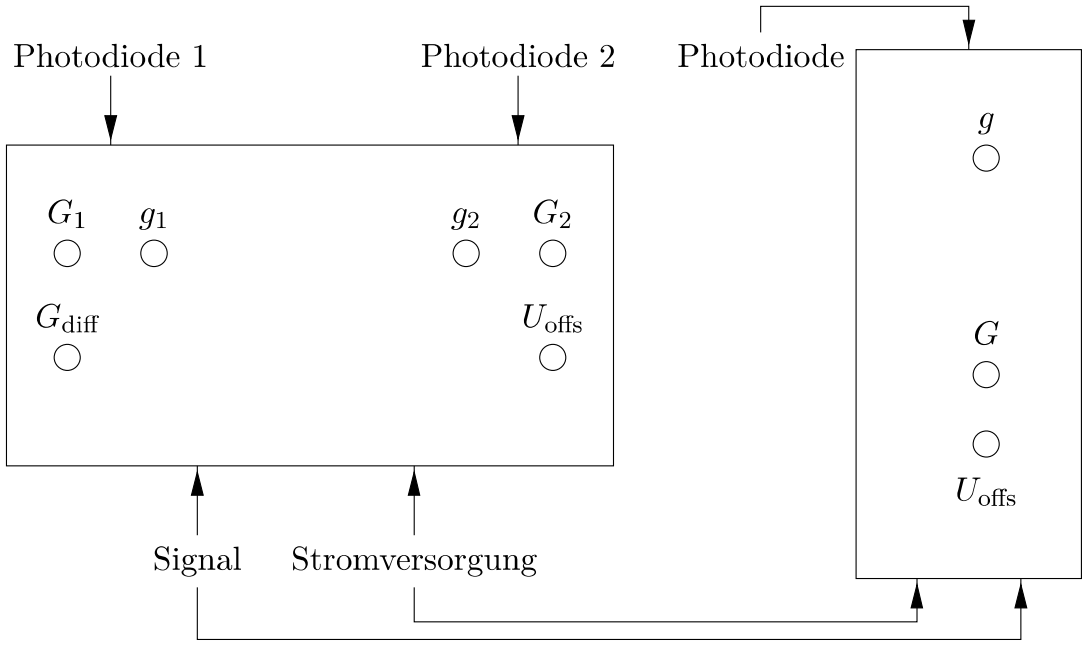

Fig. 6.5: Differential photodiode (left) and single photodiode (right).

The six rotary potentiometer of the differential photodiode are as follows (Fig. 6.5, left): the signal of the photodiode 1 is attenuated first by a factor $g_1 = 0...1$ and then amplified by $G_1 = 1...100$,the same applies to photodiode 2. Then both signals are subtracted, the difference amplifier with G_{diff} and an offset U_{offs} . The following procedure is done in order to calibrate the differential photodiode:

- g_1 and g_2 should always be set to their maximum value.
- G_1 and G_2 should be set to their minimum value.
- Both photodiodes covered e.g. with the infrared card and adjusted the offset to 0 V.
- Then G_{diff} is increased until a clear signal can be seen.
- Lastly, G_1 or G_2 increased until (approximately) getting the constant level of the signal at 0 V.
- In the case of saturation spectroscopy this stage is useful when the pump beam is covered so that both photodiodes receive the same signal and the signal can be set to zero by balancing G_1 and G_2.

The signals of the photodiodes are both plugged into the inputs of the oscilloscope, and the data acquisition card of the computer. The trigger signal of the scan control unit of the BNC port (4) is used to trigger the oscilloscope

6.2.3 Confocal Fabry-Pérot Interferometer

The confocal Fabry-Pérot interferometer has the following parameters and estimated error:

- Mirror spacing $d = (50.0 \pm 0.5)$ mm
- Reflectivity $R = 94.3\%$

In principle, the sub-beam of the Fabry-Pérot interferometer should be adjusted properly and provide a signal to the photodiode. Otherwise the lens having a focal length of $f = 100$ mm must be repositioned in front of the interferometer and coupledto the Fabry-Pérot interferometer by readjustment of the mirror to correct the beam. The resultis considered in section 6.2.4 and the photodiodes are set according to section 6.2.2.
If the transmitted intensity from the interferometer contains many different sized peaks at different positions (section 3.1), the laser is not in the single-mode operation. By adaptation of the diode current and/or the offset of the piezo control voltage, the laser can be set to the single-mode operation.

6.2.4 Recording of the absorption spectrum

Now the experimental setup for the non-pre-aligned optics is assembled, as shown in Fig. 6.1. The pump beam is initially blocked with the shutter and can be adjusted later.
In the adjustment of the non-visible laser beam to the human eye can be made visible with an infrared card. The following should be considered:

- The optical axis is ideally parallel to the table at a height of 2.5" = 63.5 mm above the mounting plate. This height must be respected everywhere.
- The laser beam should be as central as possible through the optics.
- Back reflections to the diode laser and uncontrolled reflections from surfaces especially without anti-reflective coating (infrared map, gray wedges, gas cells, and etc.) should be avoided. Always slightly tilt it in the light path.
- The polarization of the polarizing beam splitter cube must be very accurately perpendicular to the polarization of the cube from the pumping beam, so that no part of the beam can reach the diode laser. The polarizing beam splitter cube is not possible to rotate in the mounting unit.
- The focus of the lenses should be at the differential photodiode in the optically active surface of each photodiode.
- Touch optical components only on the mounting part. In case of accidental contamination of optics do not make cleaning attempts on your own, but let the supervisor know.
- The distance between the probe and reference beam should be selected such that they can be easily performed later by different halves of the double-cell gas.

When the experiment sets up properly, the correct frequency of the laser could be found at which the spectrum of the absorption spectroscopy can be seen(Fig. 2.1, top). In most cases, the laser is switched on, and is set to the single-mode operation, considerably periodically tuned in any frequency range, just not in the area of D2 line of rubidium. By small variations of the diode current and the offset of the piezo control voltage the proper frequency range must be sought. It makes sense that the spectrum does not directly begin right after the tuning points of the laser frequency, because the frequency tuning point does not follow

a linear trajectory, as can be seen at the larger distances of the first peaks in the signal of the Fabry-Pérot interferometer.

Lastly, the spectrum of absorption spectroscopy is recorded with the data acquisition card of the computer after the differential photodiode calibrated (section 6.2.2). It is important to record the signal of the Fabry-Pérot interferometer, to have a frequency scale for the evaluation of the spectra.

6.2.5 Recording of the saturation spectrum

Following the same procedure for the alignment of the pump beam is repeated to accommodate the saturation spectra. It has been found that it is useful to obtain the first spectrum from the double-cell gas. If the double gas cell associated with one half of the probe and the other half with the reference beam, wherein the pump beam is blocked, then both photodiodes of the differential photodiode should each register the same intensity and the measured difference should be zero. By a non-perfect 50-50 splitting of the beam splitter cube of the probe and reference beams as well as inaccuracies in the adjustment (may not fall all the light on the optically active surfaces of the photodiodes) the signal of a photodiode is usually greater by a certain factor than that of the other. This can be compensated by the gains G_1 and G_2 of the differential photodiode.

In addition, the pump beam is then also included, the intensities of probe-/reference- and pump beam can be adjusted. For a spectrum with well separated saturation peaks, the intensity of the pump beam must not be too large (saturation broadening!) And the probe beam must be small compared to the intensity of the pump beam to prevent saturation (Fig. 2.1, below).

Finally, the double-cell gas is again replaced by the simple gas cell, but the intensities of laser sub-beams do not require readjustment (Fig. 2.1, middle).

6.2.6 Observation of coherent dark states

The double gas cell from the previous part of the experiment is again removed and put in the cell together with the coil with μ-metal shield (against interfering magnetic fields in the vicinity of the experiment). The coil has the following parameters:

- Number of windings: $N = 380$
- Length: $l = 339.5$ mm

For its magnetic field (long coil) applies: $B = \mu_0 \frac{N}{l} I$

In the coil, the small gas cell must be located at the center of the large variation field to sample the absorption spectroscopy.Then, the balance of the differential photodiode is also as in the absorption spectroscopy. Subsequently, the frequency of the laser due to the offset of the scan control unit must be set to the ground state $F = 1$ of the Rb-87 Doppler broadening profile by successively reducing the amplitude and readjustment the offset of the scan control unit until the amplitude value equals 0. (Alternatively, Rb-85 can be used with the ground state $F = 2$, wherein the effect here is less recognizable.) The triangular wave voltage is applied to the coil that is generated by the digital-to-analog converter of the measurement board and fed through a current driver. The current I through the coil is measured by a given output of the current driver (measuring voltage U) through the data acquisition card. The measuring voltage signal will replace the photodiode signal of the interferometer at the input of the oscilloscope. The current (x axis) is plotted against the signal of the differential photodiode (y-axis). By readjustment of the offset of the scan control unit, the gain of the photodiode and the amplitude of the triangular voltage signal has to be finally optimized until a distinct peak in the center of the otherwise constant signal can be seen. Last the spectrum can again be made a recording with the PC.

For the recorded data, the following relationships are important:

- Conversions of a measured value $N \in \{\text{-}2048. \ . \ . \ , 2047\}$ of the measurement card into the appropriate voltage U: $U = \frac{N}{2048} U_{\max}$, with the maximum voltage $U_{\max}$ in the set measuring range (note it!).

- Conversion of measurement voltage U at the current driver in the coil current I: $I = 2\frac{A}{V}U$

6.3 Tasks

1. Determine the finesse of the Fabry-Pérot interferometer and compare it with the theoretical value. *The transmission spectrum of Fabry-Pérot interferometer needs to be saved for analysis.*

2. Determine the average velocity of rubidium atoms (both isotopes) in the gas cell from the liner absorption spectrum (Doppler broadened) and compare it with its theoretical value. *The transmission spectrum of Fabry-Pérot*

interferometer as well as the linear absorption spectrum of Rubidium need to be saved for analysis.

3. Assign the peaks in the spectrum of saturation spectroscopy, the transitions and crossover signals. *The transmission spectrum of Fabry-Pérot interferometer as well as the saturated absorption spectrum of Rubidium (with and without Doppler background) need to be saved for analysis.*

4. Determine the energy levels in figures 4.1 and 4.2 and distances of the energy levels using linear and Doppler free saturated absorption spectroscopy. Use the transmission spectrum of the Fabry-Pérot interferometer as a frequency scale. Compare the experimental values with the values specified in the above figures.

5. Plot the transmitted intensity from the experimentally observed coherent dark states as a function of applied magnetic field. Determine the magnetic field required to lift the degeneracy. *The periodic voltage waveform applied to the coil to generate a magnetic field and the the destroyed coherent dark states of Rubidium need to be saved for analysis.*

Bibliography

[1] Wolfgang Demtröder: Laserspektroskopie – Grundlagen und Techniken. Springer-Verlag; Berlin, Heidelberg, New York, 2000

[2] Wolfgang Demtröder: Laser Spektroscopy – Basic Concepts and Instrumentation. Springer-Verlag; Berlin, Heidelberg; second corrected printing 1981 and 1982

[3] Dieter Meschede: Optics, Light and Lasers – The Practical Approach to Modern Aspects of Photonics and Laser Physics. Wiley-VCH Verlag; Weinheim; Second, Revised and Enlarged Edition 2007

[4] Toptica Photonics AG: DL100 Diode Laser System Manual, 2005

[5] Advance Optics Laboratory "Doppler-Free Saturated Absorption Spectroscopy: Laser Spectroscopy". University of Colorado; http://massey.dur.ac.uk/resources/grad_skills/LaserSpectroscopy.pdf

[6] Thomas Rieger, Thomas Volz: "Doppler-Free Saturation Spectroscopy". Max Planck Institute for Quantum Optics; https://www.mpq.mpg.de/4992695/saturation_spectroscopy.pdf

[7] "Saturated Absorption Spectroscopy". University of Florida, 2010; http://www.phys.ufl.edu/courses/phy4803L/group_III/sat_absorbtion/SatAbs.pdf

[8] Daniel A. Steck: Rubidium 87 D Line Data. Theoretical Division, Los Alamos National Laboratory, 2003; http://george.ph.utexas.edu/~dsteck/alkalidata/rubidium87numbers.pdf

[9] Nuclear Data Evaluation Lab: Table of Nuclides. Korea Atomic Energy Research Institute, 2000; http://atom.kaeri.re.kr/